

Extremely rich dynamics from hyperchaotic Hopfield neural network: Hysteretic dynamics, parallel bifurcation branches, coexistence of multiple stable states and its analog circuit implementation

Z. Tabekoueng Njitacke^{1,2,a}, Sami Doubla Isaac^{2,3}, J. Kengne²,
A. Nguomkam Negou^{2,3}, and Gervais Dolvis Leutcho^{2,3}

¹ Department of Electrical and Electronic Engineering, College of Technology (COT), University of Buea, P.O. Box 63, Buea, Cameroon

² Unité de Recherche d'Automatique et Informatique Appliquée (URAlA), Department of Electrical Engineering, IUT-FV Bandjoun, University of Dschang, Bandjoun, Cameroon

³ Unité de Recherche de Matière Condensée, d'Electronique et de Traitement du Signal (URMACETS), Department of Physics, University of Dschang, University of Dschang, P.O. Box 67, Dschang, Cameroon

Received 22 September 2019 / Received in final form 4 November 2019
Published online 26 March 2020

Abstract. In this work, we investigate the dynamics of a model of 4-neurons based hyperchaotic Hopfield neural network (HHNN) with a unique unstable node as a fixed point. The basic properties of the model including symmetry, dissipation, and condition of the existence of an attractor are explored. Our numerical simulations highlight several complex phenomena such as periodic orbits, quasi-periodic orbits, and chaotic and hyperchaotic orbits. More interestingly, it has been revealed several sets of synaptic weights matrix for which the HHNN studied display multiple coexisting attractors including two, three and four symmetric and disconnected attractors. Both hysteretic dynamics and parallel bifurcation branches justify the presence of these various coexisting attractors. Basins of attraction with the riddle structure of some of the coexisting attractors have been computed showing different regions in which each solution can be captured. Finally, PSpice simulations are used to further support the results of our previous analyses.

1 Introduction

Dynamical systems theory is a powerful tool to explain and predict complex dynamics in applications by analyzing appropriate mathematical models [1]. Indeed mathematical models are used in natural and engineering disciplines, as well as in social sciences. A mathematical model may help to explain a system's behavior, to study the effects of different components, and to make predictions. Several mathematical

^a e-mail: zerictabekoueng@yahoo.fr

models are found in the literature including, diseases model (Cancer and HIV/AIDS) [2], electrical machine model, atmospheric model [3,4], satellite model [5], financial model [6], calcium oscillation model [7], neurons model [8–10] and laser model [11–13] just to name few. Many artificial neural networks have been presented to simulate the chaotic or hyperchaotic dynamics of the brain. Recently, some numerical and experimental investigations of chaotic dynamics in Hopfield networks have been addressed [14–24]. Results revealed some striking behaviors including chaotic orbits with both single scroll and double scroll, quasi-periodic orbits, hyperchaotic orbits, transient behaviors, antimonotonicity, and coexistence of bifurcations with multiple stable states [9,10,14–18]. This latter phenomenon is widely known as multistability; means the coexistence of several types of attractors in a given system for the same set of parameters, starting from different initial conditions. This widespread phenomenon has already been found in several classes of dynamical systems such as chemical, mechanical, electrical, ecological biological systems and so on [14–24]. For example, Lai et al. [25] introduced a novel three-dimensional chaotic system with three nonlinearities. A salient feature of that novel system was its ability to display the coexistence of multiple attractors caused by different initial values. With the change of parameters, the authors found that the system was able to experience mono-stability, bi-stability, mono-periodicity, bi-periodicity, one strange attractor, and two coexisting strange attractors. The complex dynamic behaviors of the system were revealed by analyzing the corresponding equilibria and using the numerical simulation method. Besides, an electronic circuit was given for implementing the chaotic attractors of the system. Using the introduced chaotic system, the S-Box was developed for cryptographic operations. Similar types of analyses, as well as application, have been done by Lai et al. [26] during the investigation of an extended Lü system. Recently, Lai et al. [27] have reported a method for constructing multiple coexisting attractors from a chaotic system. Exploiting that technique, a new four-dimensional chaotic system with only one equilibrium and two coexisting strange attractors was established. Also, they show that the core of their method was to batch replicate the attractor of the system in phase space via generating multiple invariant sets and the generation of invariant sets depends on the equilibria, which can be extended by using some simple functions with multiple zeros. Very recently the same research group [28] constructed an extremely simple chaotic system with infinitely many coexisting chaotic attractors. The phenomenon of coexisting attractors of the new system was numerically investigated. Finally, circuit and microcontroller-based implementation of the system was presented as well.

Concerning the coexistence of stable states in neuronal models particularly in Hopfield neural networks, several works have already been proposed [14,15,23,24]. Bao and collaborators [14] found the coexistence of three different asymmetric attractors with different shapes in a model of HNN based on hyperbolic-type memristor. Respectively, the authors also found the coexistence of up to four disconnected attractors in a simplified 3D HNN [15]. In the investigations of Bao, results have been perfectly supported via various experimental studies. Njitacke and colleagues [23,24], have highlighted the coexistence of up to six disconnected stable states and the phenomenon of antimonotonicity in several models of HNN. Among these neuronal models, some were built with nonlinear synaptic weights [14,23,24] while others were built with linear synaptic weights [15,29,30]. Very recently Bao et al. have explored the dynamical effects of neuron activation gradient on the dynamics of a Hopfield neural network through numerical analyses and hardware experiments [29]. Their results demonstrate that complex dynamical behaviors associated with the neuron activation gradient emerge in the HNN model, including coexisting limit cycle oscillations, coexisting chaotic spiral attractors, chaotic double scrolls, forward and reverse period-doubling cascades, and crisis scenarios.

From these aforementioned works, several complex behaviors such as antimonotonicity and coexistence of bifurcations with multiple stable states have been found during the investigations of a chaotic HNN. However such rich dynamical behaviors have not yet been revealed in hyperchaotic one thus, it deserves to be explored. To shed more light on that thinking, we address the nonlinear dynamics of a hyperchaotic Hopfield neural network with linear synaptic weight matrix based on the following objectives:

- (a) To carry out a systematic analysis of HHNN under investigation and explain the chaos and hyperchaotic mechanisms;
- (b) To define the set of the synaptic weight matrices in which the model experiences multiple coexisting chaotic and hyperchaotic attractors, hysteretic dynamics and parallel bifurcations;
- (c) To carry out a series of PSpice simulations of the model of HHNN to support the theoretical predictions.

Some interests of this study are related to the fact that Hopfield neural networks can model brain dynamics [31], they can be applied in stereo matching [32] or associative memory [33]. Indeed there are several works focused on the dynamics of the Hopfield neural network with various types of coexisting bifurcations. However, these various works are focused only on the chaotic HNN. Then is no case of coexisting attractors addressed on HHNN hence the interest of this work. Besides the coexisting attractors found in this work are all symmetric in contrast to the previous works addressed in HNN where the coexisting attractors appeared in symmetric pairs [14,15,23,24,28].

The rest of this scientific contribution is structured as follows: In Section 2, the presentation and description of the HHNN are performed. Analyses are carried out in terms of dissipation analysis with the condition of the existence of attractors and the analysis of the stability of the unique stationary point. In section 3, Traditional analysis tools are exploited to highlight various regular and irregular behaviors including the coexistence of multiple stable states. In Section 4, a series of PSpice explorations are carried out to support our previous analysis. Finally, some concluding remarks and proposals for future work are provided in Section 5.

2 Description of the HHNN

2.1 Mathematical expression of the model of HHNN

Chaotic or hyperchaotic Hopfield neural networks are generally used to describe some brain process such the context of learning and memory. In such type of neuron, the circuit equation can be described as

$$\dot{x}_i = -c_i x_i + \sum_{j=1}^n w_{ij} \tanh(x_j) + I_i. \quad (1)$$

In equation (1), x_i is a state variable of the neuron c_i is the membrane resistance between the inside and outside of the neuron, I_i is the input bias current. The matrix $W = w_{ij}$ is a $n \times n$ synaptic weight matrix showing the strength of connections between neurons [14–18]. The $\tanh(x_j)$ is the smooth nonlinear activation function indicating the voltage input from the j -th neuron. In this contribution, we consider that, $I_i = 0$ and $n = 4$. Based on these various hypotheses, we investigate the hyperchaotic Hopfield neural networks with the topological connection depicted in Figure 1. From this general topological connection, the synaptic weight matrix of equation (1) is proposed.

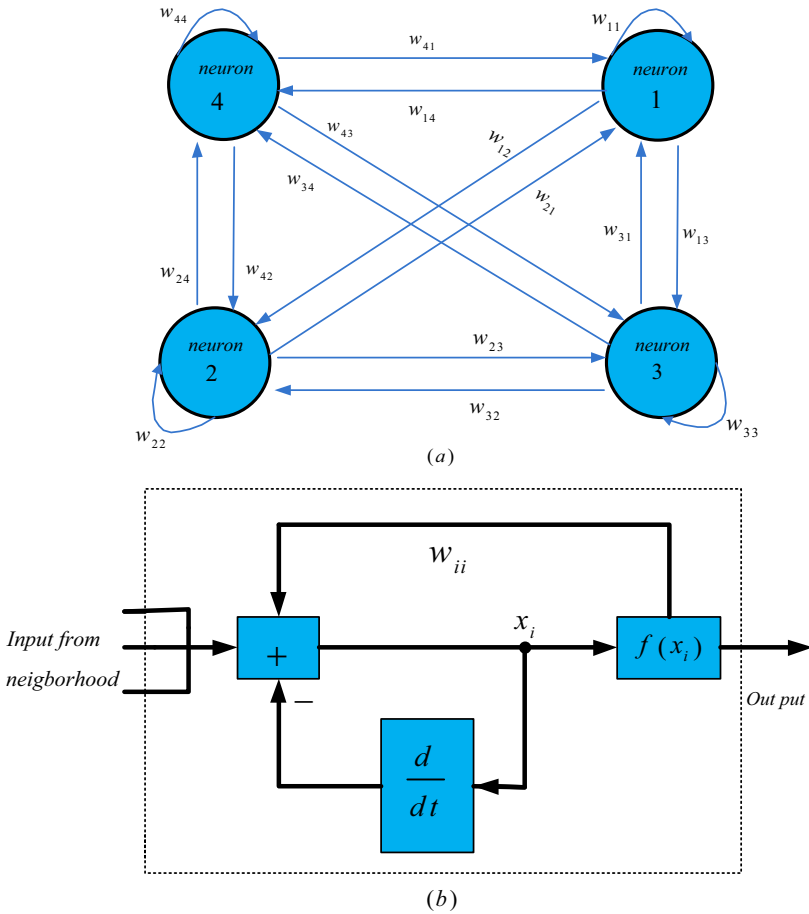


Fig. 1. Topological connection of the hyper-chaotic Hopfield neural network (HHNN) in (a); the detail diagram of a neuron in (b).

$$W = \begin{bmatrix} w_{11} & w_{12} & w_{13} & w_{14} \\ w_{21} & w_{22} & w_{23} & w_{24} \\ w_{31} & w_{32} & w_{33} & w_{34} \\ w_{41} & w_{42} & w_{43} & w_{44} \end{bmatrix} = \begin{bmatrix} 1 & 0.5 & -3 & -1 \\ 0 & w_{22} & 3 & 0 \\ 3 & -3 & w_{33} & 0 \\ 100 & 0 & 0 & w_{44} \end{bmatrix} \quad (2a)$$

$$c = [1 \ 1 \ 1 \ 100]^T. \quad (2b)$$

From the above considerations, the smooth nonlinear fourth order differential equations describing the dynamics of the proposed 4-neurons based HHNN are taken in a dimensionless form as:

$$\begin{cases} \dot{x}_1 = -x_1 + \tanh(x_1) + 0.5 \tanh(x_2) - 3 \tanh(x_3) - \tanh(x_4) \\ \dot{x}_2 = -x_2 + w_{22} \tanh(x_2) + 3 \tanh(x_3) \\ \dot{x}_3 = -x_3 + 3 \tanh(x_1) - 3 \tanh(x_2) + w_{33} \tanh(x_3) \\ \dot{x}_4 = -100x_4 + 100 \tanh(x_1) + w_{44} \tanh(x_4) \end{cases} \quad (3)$$

Referring to equation (3), there are three synaptic weights (w_{22} , w_{33} and w_{44}) from which the behavior of the HHNN model can be investigated.

2.2 Dissipation, condition of existence of attractors and symmetry

The volume contraction rate is the main quantity used to evaluate the dissipation property of a given dynamical system [34,35]. System (3) can be written in the following vector notation

$$\frac{d\varphi}{dt} = f(\varphi) = \begin{bmatrix} f_1(x_1, x_2, x_3, x_4) \\ f_2(x_1, x_2, x_3, x_4) \\ f_3(x_1, x_2, x_3, x_4) \\ f_4(x_1, x_2, x_3, x_4) \end{bmatrix} \tag{4}$$

with

$$\begin{cases} f_1(x_1, x_2, x_3, x_4) = -x_1 + \tanh(x_1) + 0.5 \tanh(x_2) - 3 \tanh(x_3) - \tanh(x_4) \\ f_2(x_1, x_2, x_3, x_4) = -x_2 + w_{22} \tanh(x_2) + 3 \tanh(x_3) \\ f_3(x_1, x_2, x_3, x_4) = -x_3 + 3 \tanh(x_1) - 3 \tanh(x_2) + w_{33} \tanh(x_3) \\ f_4(x_1, x_2, x_3, x_4) = -100x_4 + 100 \tanh(x_1) + w_{44} \tanh(x_4) \end{cases} \tag{5}$$

Now considering any space Ω in \mathbb{R}^4 with a smooth boundary, satisfying $\Omega(t) = \Phi_L(t)$ where $\Phi_L(t)$ is the flow of f . Considering $V(t)$ denotes the volume of $\Omega(t)$. Using Liouville's theorem, we obtain:

$$\frac{dV}{dt} = \int_{\Omega(t)} (\nabla \cdot f) dx_1 dx_2 dx_3 dx_4 \tag{6}$$

where $(\nabla \cdot f)$ represents the volume contraction rate. It can be easily checked that, this volume is equal:

$$\nabla \cdot f = -103 + w_{11} \text{sech}^2(\bar{x}_1) + w_{22} \text{sech}^2(\bar{x}_2) + w_{33} \text{sech}^2(\bar{x}_3) + w_{44} \text{sech}^2(\bar{x}_4) \tag{7}$$

since that $-1 < \tanh(\bar{x}_i) < 1$ for all $x_i (i = 1, \dots, 4)$ with an appropriate choice of synaptic weights w_{11} , w_{22} and w_{33} our model can be dissipative and support attractors. We recall that the dissipation property of a system gives the presence of bounded global attractor and an analytical indication of the global attractor in the phase space [34,35] The confinement of the neuronal model can be supported using the approach described in [36,37]. A Lyapunov function is introduced as

$$V(x_1, x_2, x_3, x_4) = \frac{1}{2}x_1^2 + \frac{1}{2}x_2^2 + \frac{1}{2}x_3^2 + \frac{1}{2}x_4^2. \tag{8}$$

The corresponding time derivative of the Lyapunov function candidate is given as

$$\begin{aligned} \dot{V}(x_1, x_2, x_3, x_4) &= x_1\dot{x}_1 + x_2\dot{x}_2 + x_3\dot{x}_3 + x_4\dot{x}_4 \\ &= -(x_1^2 + x_2^2 + x_3^2 + 100x_4^2) + \tanh(x_1)(x_1 + 3x_3 + 100x_4) \\ &\quad + \tanh(x_2)(0.5x_1 + w_{22}x_2 - 3x_3) + \tanh(x_3) \\ &\quad \times (-3x_1 + 3x_2 + w_{33}x_3) + \tanh(x_4)(-x_1 + w_{44}x_4) \end{aligned} \tag{9}$$

considering that

$$\begin{aligned} v(x_1, x_2, x_3, x_4) &= \tanh(x_1)(x_1 + 3x_3 + 100x_4) + \tanh(x_2)(0.5x_1 + w_{22}x_2 - 3x_3) \\ &\quad + \tanh(x_3)(-3x_1 + 3x_2 + w_{33}x_3) + \tanh(x_4)(-x_1 + w_{44}x_4) \end{aligned} \tag{10}$$

Equation (9) can be then transformed as

$$\dot{V} = -\alpha V(x_1, x_2, x_3, x_4) + v(x_1, x_2, x_3, x_4) \tag{11}$$

where α is a positive constant. Based on the fact that, $\tanh(x_i) < 1$ for all x_i ($i = 1, \dots, 4$) thus, equation (10) can be reduced as

$$\begin{aligned}
 v(x_1, x_2, x_3, x_4) &\leq |\tanh(x_1)(x_1 + 3x_3 + 100x_4)| + |\tanh(x_2)(0.5x_1 + w_{22}x_2 - 3x_3)| \\
 &\quad + |\tanh(x_3)(-3x_1 + 3x_2 + w_{33}x_3)| + |\tanh(x_4)(-x_1 + w_{44}x_4)| \\
 &< |(x_1 + 3x_3)| + |(0.5x_1 + w_{22}x_2 - 3x_3)| \\
 &\quad + |(-3x_1 + 3x_2 + w_{33}x_3)| + |(-x_1 + w_{44}x_4)| \\
 &\leq 5.5|x_1| + (w_{22} + 3)|x_2| + (w_{33} + 6)|x_3| + (w_{44} + 100)|x_4|
 \end{aligned} \tag{12}$$

Let $D_0 \geq 0$ be the sufficiently large region. For all (x_1, x_2, x_3, x_4) satisfying $V(x_1, x_2, x_3, x_4) = D$ with $D > D_0$ there exists the following inequality

$$\begin{aligned}
 v(x_1, x_2, x_3, x_4) &< 5.5|x_1| + (w_{22} + 3)|x_2| + (w_{33} + 6)|x_3| + (w_{44} + 100)|x_4| \\
 &< x_1^2 + x_2^2 + x_3^2 + 100x_4^2 = \alpha V(x_1, x_2, x_3, x_4)
 \end{aligned} \tag{13}$$

then, on the surface

$$\{(x_1, x_2, x_3, x_4) | V(x_1, x_2, x_3, x_4) = D\} \tag{14}$$

with $D > D_0$ there yields

$$\dot{V} = -\alpha V(x_1, x_2, x_3, x_4) + v(x_1, x_2, x_3, x_4) < 0. \tag{15}$$

Consequently, the set

$$\{(x_1, x_2, x_3, x_4) | V(x_1, x_2, x_3, x_4) \leq D\} \tag{16}$$

is a bounded region of all solutions of the model of hyperchaotic Hopfield neural networks. It is obvious that equation (3) is invariant under the coordinate’s permutation $(x_1, x_2, x_3, x_4) \rightarrow (-x_1, -x_2, -x_3, -x_4)$ meaning that the model is symmetric with respect to the origin. So attractors of the model will appear in symmetric pair to restore the exact symmetry of the model by using a pair of symmetric initial conditions. Otherwise the attractors generated will remain symmetric if the exact symmetry of the orbits has already been restored.

2.3 Analysis of the eigenvalues

To obtain the equilibrium points of our model, let $\dot{x}_1 = \dot{x}_2 = \dot{x}_3 = \dot{x}_4 = 0$; referring to the work of [9] and set of synaptic weights matrices of equation (3) the model of HHNN under consideration has a unique equilibrium point which is the origin $E_0 = (0, 0, 0, 0)$. The Jacobian matrix at that unique equilibrium point can be easily given as follows.

$$J = \begin{bmatrix} -1 + \text{sech}^2(\bar{x}_1) & 0.5\text{sech}^2(\bar{x}_2) & -3\text{sech}^2(\bar{x}_3) & -\text{sech}^2(\bar{x}_4) \\ 0 & -1 + w_{22}\text{sech}^2(\bar{x}_2) & 3\text{sech}^2(\bar{x}_3) & 0 \\ 3\text{sech}^2(\bar{x}_1) & -3\text{sech}^2(\bar{x}_2) & -1 + w_{33}\text{sech}^2(\bar{x}_3) & 0 \\ 100\text{sech}^2(\bar{x}_1) & 0 & 0 & -100 + w_{44}\text{sech}^2(\bar{x}_4) \end{bmatrix} \tag{17}$$

where $\text{sech}^2(\bar{x}_i) = (1 - \tanh^2(\bar{x}_i))$ with $i = 1, \dots, 4$ is the derivative of the nonlinear activation function of each neuron at the equilibrium point \bar{x}_i . self-synaptic weight of the second the third and fourth neuron are given in the next section. The eigenvalues at the origin are obtained by solving the following characteristic equation:

$$\det(\lambda I - J) = \lambda + a_1\lambda + a_2\lambda + a_3\lambda + a_4 = 0 \tag{18}$$

Table 1. Eigenvalues and stability of the unique equilibrium point computed for some discrete values of self-synaptic weights.

Figure of which parameters are used	Eigen values at origin	Nature of Eigen values
Figures 6a and 3	78.7317 1.3827 0.4428 ± 4.2416i	Unstable node
Figures 6b and 3	88.8761 1.3097 0.4071 ± 4.2432i	Unstable focus
Figures 8 and 2	68.5438 1.2764 0.3799 ± 4.2332i	Unstable focus
Figures 9 and 2	68.5438 1.1904 0.3329 ± 4.2271i	Unstable focus

$$\begin{cases}
 a_1 = 103 - bw_{22} - cw_{33} - dw_{44} - a \\
 a_2 = 9ac - 102a + 100ad + 9bc - 102bw_{22} - 102cw_{33} - 3dw_{44} + abw_{22} + \\
 acw_{33} + adw_{44} + bcw_{22}w_{33} + bdw_{22}w_{44} + cdw_{33}w_{44} + 303 \\
 a_3 = 909ac - 201a + 200ad + 909bc - 201bw_{22} - 201cw_{33} - 3dw_{44} - (27abc)/2 + \\
 101abw_{22} + 101acw_{33} + 2adw_{44} + 101bcw_{22}w_{33} + 2bdw_{22}w_{44} + 2cdw_{33}w_{44} - \\
 9abcw_{22} - 100abdw_{22} - 100acd w_{33} - 9acd w_{44} - 9bcd w_{44} - abcw_{22}w_{33} - \\
 abdw_{22}w_{44} - acdw_{33}w_{44} - bcdw_{22}w_{33}w_{44} + 301 \\
 a_4 = 900ac - 100a + 100ad + 900bc - 100bw_{22} - 100cw_{33} - dw_{44} - 1350abc + \\
 100abw_{22} + 100acw_{33} + adw_{44} + 100bcw_{22}w_{33} + bdw_{22}w_{44}cdw_{33}w_{44} + \\
 900abcd - 900abcw_{22} - 100abdw_{22} - 100acd w_{33} - 9acd w_{44} - 9bcd w_{44} + \\
 (27abcd w_{44})/2 - 100abcw_{22}w_{33} - abdw_{22}w_{44} - acdw_{33}w_{44} + 100abcdw_{22}w_{33} + \\
 9abcdw_{22}w_{44} - bcdw_{22}w_{33}w_{44} + abcdw_{22}w_{33}w_{44} + 100
 \end{cases} \tag{19.a}$$

where

$$a = \operatorname{sech}^2(\bar{x}_1), \quad b = \operatorname{sech}^2(\bar{x}_2), \quad c = \operatorname{sech}^2(\bar{x}_3) \quad \text{and} \quad d = \operatorname{sech}^2(\bar{x}_4). \tag{19.b}$$

The coefficients of the polynomial (Eq. (18)) are all nonzero. According to the Routh–Hurwitz criterion, the real parts of the roots of equation (18) are positive if and only if the following inequalities are satisfied:

$$\begin{aligned}
 &a_1 > 0 \\
 &a_1 a_2 - a_3 > 0 \\
 &a_1 (a_2 a_3 - a_1 a_4) - a_3^2 > 0 \\
 &a_4 > 0
 \end{aligned} \tag{20}$$

Now, considering some values of synaptic weights connection described by equation (2); the four conditional inequalities of equation (20) at different synaptic weights w_{22} and w_{44} are found by numerical simulations (see Tab. 1). As a result, it can be seen that the origin $E_0(0, 0, 0, 0)$ which is the unique stationary point is an unstable node with two complex conjugate roots with positive real parts, two positive real roots for some discrete values of the synaptic weights provided in Table 1. Therefore, we conclude that the model hyperchaotic Hopfield neural networks investigated experiences self-excited orbits [16–22].

3 Complex dynamics of the HHNNs

In this section, all the simulations are made in Turbo Pascal software using the fourth-order Runge-Kutta formula with a constant time grid of $\Delta t = 2 \times 10$. Synaptic weights are chosen in extended precision mode using trial and error approach in order to generate complex behaviors including chaotic or hyperchaotic ones. Quantitative and qualitative nonlinear analysis tools such as graph of Lyapunov spectrum using Wolf algorithm [38], bifurcation diagrams, phase portraits, Poincaré sections as well as frequency spectra are used to explore regions in the parameter space in which the HHNN exhibits regular and irregular behaviors.

3.1 Transition between regular and irregular behavior in the model

Obviously, regular behavior in a dynamical system is characterized by different periodicity. For example, a dynamical regime with periodic motion is regular and thus coherent. A chaotic regime that can be also viewed as noise according to the time series is strongly irregular and therefore incoherent. Main diagnostic tools used to measure regular or irregular behavior in a given nonlinear dynamical system are Lyapunov exponents graphs and bifurcation diagrams. For instance in Figures 2b and 3b, a regular dynamic is characterized by null Lyapunov exponent λ_1 . However, this analysis tool is unable to give an exact period of the system for a specific set of parameters. Bifurcation diagrams plotted, generally combined with the graph of Lyapunov exponent is the best tool used to overcome this drawback. From bifurcation diagrams of Figures 2a and 3a, the periodicity is obtained by counting the number of local maxima/minima shaped on diagrams. The dynamics with regular behavior is characterized by a countable number of local maxima/minima. The dynamic regime with an incoherent/irregular behavior is localized by an infinite (uncountable) number of local maxima/minima (see Figs. 2 and 3). Sometimes, one might think that the bifurcation exhibits an irregular behavior characterized by a thick diagram whereas it is not the case. Such type of behavior is known as quasiperiodic orbits (torus behavior) characterized by two null Lyapunov exponents.

To understand the global dynamic behavior of the HHNN investigated, we have provided Table 2 which gives the general meaning of Lyapunov exponent's plots of Figures 2 and 3. From that Table 2 and various graphs shaped in Figures 2 and 3, the model of neuron investigated in this scientific contribution exhibits regular motions including periodic orbits with different periodicities and 2-torus. Besides the coherent (regular) behavior, the studied model displays incoherent (irregular) behaviors including chaos and hyperchaos. From these several bifurcations plotted, some windows can be observed where the traced evolve with a hopping manner. These windows represent regions where the model develops the coexistence of multiple attractors associated either to hysteresis or parallel bifurcations. The general behavior of the model investigated in this work is shown in the two parameter bifurcation depicted in Figure 4. When w_{22} and w_{33} are varied simultaneously, five sets of data are displayed: we have static behavior characterized by a point attractors (blue and cyan), periodic orbits and quasiperiodic orbits (yellow), chaotic orbits (red) and hyperchaotic orbits (brown). Because of the dependency of the initial conditions (multistable property), the structure of the two parameters diagram can change if it is computed again starting from different initial points.

Remark that for all the bifurcation diagrams computed in paper, of any discrete value of the synaptic weights, the computed periodic, chaotic or hyperchaotic orbits appear under a symmetric form. This symmetric nature of the orbits is related to conditional symmetry reported in several works [39–41] but to the fact, the set of

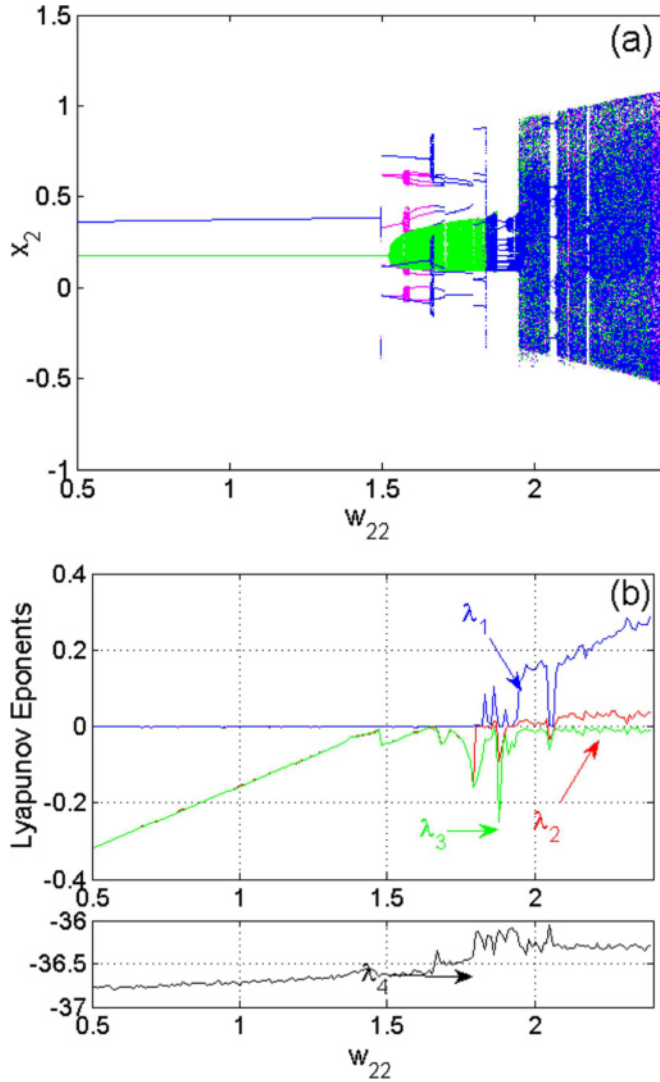


Fig. 2. Bifurcation diagram (a) showing local maxima of the neuron x_2 versus parameter w_{22} and the corresponding graph (b) of Lyapunov exponents λ_i plotted in the range $0.5 \leq w_{22} \leq 2.5$. These superimposed bifurcation diagrams are obtained with initial condition: $(x_1(0), x_2(0), x_3(0), x_4(0))$ are $(0.01, -0.02, 0, 0)$. Magenta and green respectively in the diagram are obtained by increasing respectively decreasing the synaptic weight w_{22} while the one in blue is obtained for increasing the control parameter, starting from the same fixed initial condition $(0.01, -0.02, 0, 0)$. Others synaptic weights are $w_{11} = 1, w_{12} = 0.5, w_{13} = -3, w_{14} = -1, w_{21} = 0.0, w_{23} = 3, w_{24} = 0, w_{31} = 3, w_{32} = -3, w_{33} = 1, w_{34} = 0, w_{41} = 100, w_{42} = 0, w_{43} = 0, w_{44} = 170, c_1 = c_2 = c_3 = 1, c_4 = 100$.

synaptic weights used in this work does not enable the HHNN to undergo the phenomenon of symmetry breaking during bifurcation process.

In addition Li and Yang [12] present the coexistence of two asymmetric orbits in a simplified Hopfield-type neural network with piece-wise linear (PWL) activation functions. Remark that PWL activation functions have the advantage that it can be solved analytically. However, it represents only a first-order description

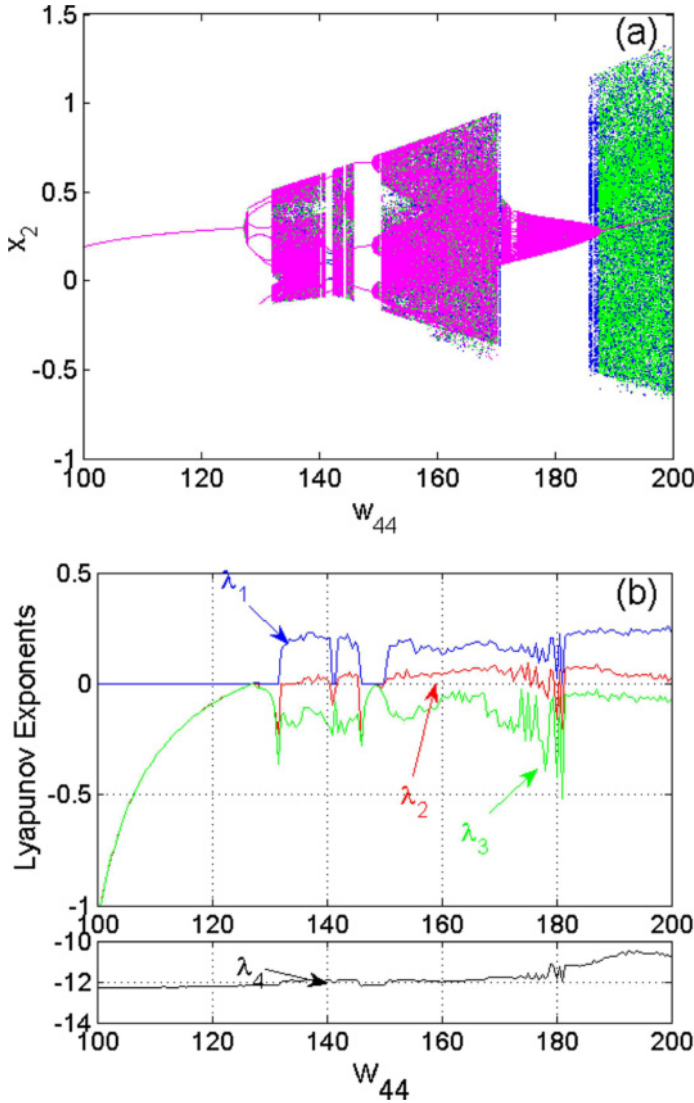


Fig. 3. Bifurcation diagram (a) showing local maxima of the neuron x_2 versus parameter w_{44} and the corresponding graph (b) of Lyapunov exponents λ_i plotted in the range $100.0 \leq w_{44} \leq 200.0$. These superimposed bifurcation diagrams are obtained with initial condition: $(x_1(0), x_2(0), x_3(0), x_4(0))$ are $(0.01, -0.02, 0, 0)$. The magenta and green in the diagram respectively are obtained by increasing respectively decreasing the synaptic weight w_{44} while the one in blue is obtained for increasing the control parameter, starting from the same fixed initial condition $(0.01, -0.02, 0, 0)$. Others synaptic weights are $w_{11} = 1, w_{12} = 0.5, w_{13} = -3, w_{14} = -1, w_{21} = 0.0, w_{22} = 2, w_{23} = 3, w_{24} = 0, w_{31} = 3, w_{32} = -3, w_{33} = 1, w_{34} = 0, w_{41} = 100, w_{42} = 0, w_{43} = 0, c_1 = c_2 = c_3 = 1, c_4 = 100$.

(i.e. qualitative description) of the neuronal model and consequently may lead to erroneous bifurcations in the real physical systems. In contrast, a smooth mathematical model of the activation functions can be exploited for a better characterization of both coherent and incoherent behaviors of the model [16–19]. This latter approach has been used in several works that focused on the multistable properties of the

Table 2. Attractors generated depending of Lyapunov exponents values.

Nature of Lyapunov exponents	Attractors type
$\lambda_{1,2,3,4} < 0$	Point
$\lambda_1 = 0$ and $\lambda_{2,3,4} < 0$	Limit cycle (periodic orbits)
$\lambda_{1,2} = 0$ and $\lambda_{3,4} < 0$	For 2-torus (quasiperiodic orbits)
$\lambda_{1,2,3} = 0$ and $\lambda_4 < 0$	For 3-torus
$\lambda_1 > 0$, $\lambda_2 = 0$ and $\lambda_{3,4} < 0$	Chaotic orbits
$\lambda_{1,2} > 0$, $\lambda_3 = 0$ and $\lambda_4 < 0$	For hyperchaotic orbits

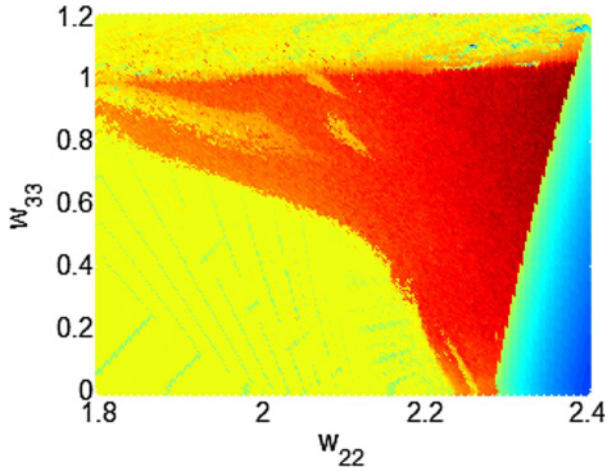


Fig. 4. Standard Lyapunov stability diagrams in the (w_{22}, w_{33}) plane obtained by scanning upward the values of control parameters where Lyapunov exponents are unable to discriminate individual oscillatory phases: the blue and cyan shadings mark the non-oscillation, yellow for periodic and quasiperiodic oscillations, red color denotes chaos and brown for hyperchaotic behavior respectively. Initial conditions are $(0.01, -0.02, 0, 0)$.

HHNN [14,15,23,24,28] but not hyperchaotic one. This is if we reconsider this work by using piece-wise linear (PWL) activation functions in an HHNN the obtained results should be completely different.

3.2 Coexistence of bifurcations and multiple attractors

Many dynamical systems can exhibit many coexisting stable states for a same set of parameters. This widespread phenomenon in nature is called multistability. This phenomenon has been found in several separated branches of science, including climate science, physics, chemistry, ecology, biology, neuroscience, and genetics [14–24]. When a coexistence of a multitude of states is observed, the system can switch from one stable state to the other either randomly by perturbations or in a desired manner using a control strategy [42]. To better observe the phenomenon of coexistence of stable states in the model investigated, we have provided Figure 5 which is an extension of the diagram in Figure 2 in the range $0.5 \leq w_{22} \leq 2.5$. From this diagram, the coexistence of several stable states with different natures can be observed including periodic, torus, chaotic and hyperchaotic attractors. For example in Figure 3a when $w_{44} = 180$ (resp. $w_{44} = 190$) the model under consideration displays coexistence of quasiperiodic orbits (magenta) and chaotic (black) orbits. Respectively, coexistence

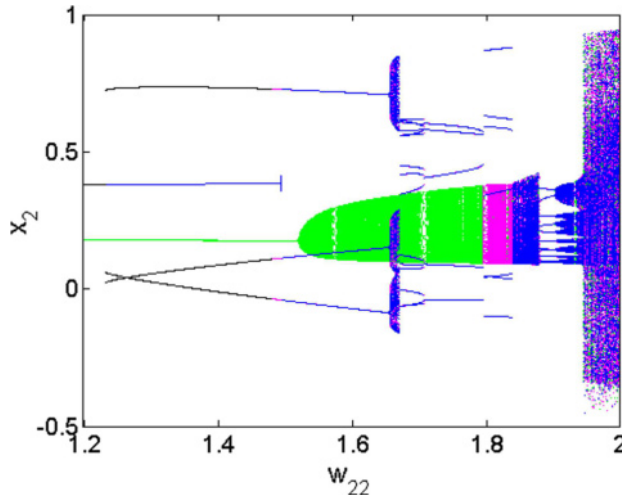


Fig. 5. Enlargement of the bifurcation diagram of Figure 2 showing the region in which the Hopfield neural network exhibits multiple coexisting attractors. This region corresponds to values of synaptic weight w_{22} in the range $1.2 \leq w_{22} \leq 2$. Four sets of data are superimposed corresponding, respectively, for increasing and decreasing the synaptic weight w_{22} (see Tab. 3).

Table 3. Different procedures used to obtain coexisting bifurcation diagrams for varying w_{22} (see Fig. 7). The rest of parameters are fixed as follows: Other parameters are $w_{11} = 1, w_{12} = 0.5, w_{13} = -3, w_{14} = -1, w_{21} = 0.0, w_{23} = 3, w_{24} = 0, w_{31} = 3, w_{32} = -3, w_{33} = 1, w_{43} = 0, w_{41} = 100, w_{42} = 0, w_{43} = 0, w_{44} = 170, c_1 = c_2 = c_3 = 1, c_4 = 100$.

Color graph	Parameter range	Sweeping direction	Initial conditions ($X_1(0), X_2(0), X_3(0), X_4(0)$)
Green	$1.48 \leq w_{22} \leq 2$	Increasing	(0, 1, 0, 0)
	$1.2 \leq w_{22} \leq 1.48$	Decreasing	(0, 1, 0, 0)
Magenta	$1.48 \leq w_{22} \leq 2$	Increasing	(0, 0.8, 0, 0)
	$1.2 \leq w_{22} \leq 1.48$	Decreasing	(0, 0.8, 0, 0)
Black	$1.48 \leq w_{22} \leq 2$	Increasing	(0, 0.6, 0, 0)
	$1.2 \leq w_{22} \leq 1.48$	Decreasing	(0, 0.6, 0, 0)
Blue	$1.48 \leq w_{22} \leq 2$	Increasing	(0, 0.4, 0, 0)
	$1.2 \leq w_{22} \leq 1.48$	Decreasing	(0, 0.4, 0, 0)

of period-1 limit cycle (magenta) and hyperchaotic (black) attractors is as depicted in Figures 6a(i) and 6b(i). On the same figures, hyperchaotic orbits are characterized by a large number of points on the Poincaré map. Periodic orbit has a finite number of points on the Poincaré map and quasiperiodic orbits are characterized by points gathering like circles (see Figs. 6a(ii) and 6b(ii)).

These singular cases of the coexisting orbits in a HHNN are supported using basins of attraction (see Fig. 7). In Figure 7a the basins of attraction with very complex shape having a riddle structure justify the higher sensibility of the model to initial conditions in that range of system parameters. In contrast, the one in Figure 7b presents a very simple structure since each attractor processes a specific region where their basin of attraction is located. Likewise, the coexistence of several regular stable states can be also captured as represented in Figures 8 and 9. For example, Figure 8a(i) displays the

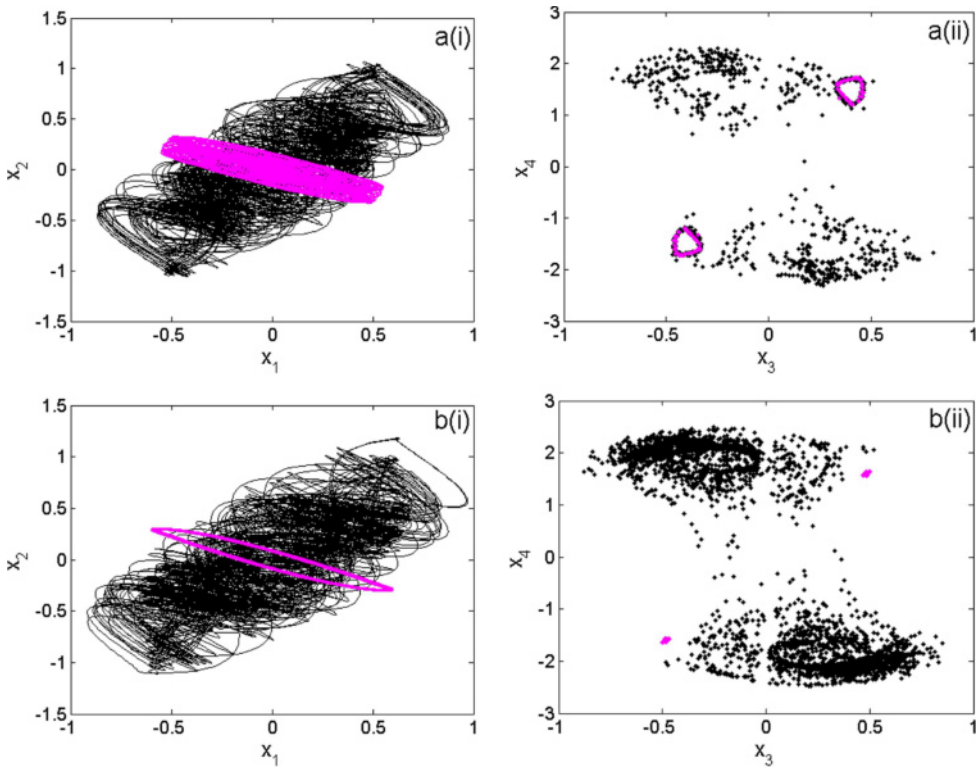


Fig. 6. Coexistence of two different attractors with different shape. (a) corresponds to a symmetric torus and symmetric chaotic attractor for $w_{44} = 180$, Initial conditions $(x_1(0), x_2(0), x_3(0), x_4(0))$ are $(0, 1, 0, 0)$ and $(0, 0.6, 0, 0)$ respectively, with their corresponding double sided Poincaré section. (b) corresponds to a symmetric period-1 and symmetric hyper-chaotic attractor for $w_{44} = 190$, Initial conditions $(x_1(0), x_2(0), x_3(0), x_4(0))$ are $(0, 2.24, 0, 0)$ and $(0, 1, 0, 0)$ respectively, with their corresponding double sided Poincaré section.

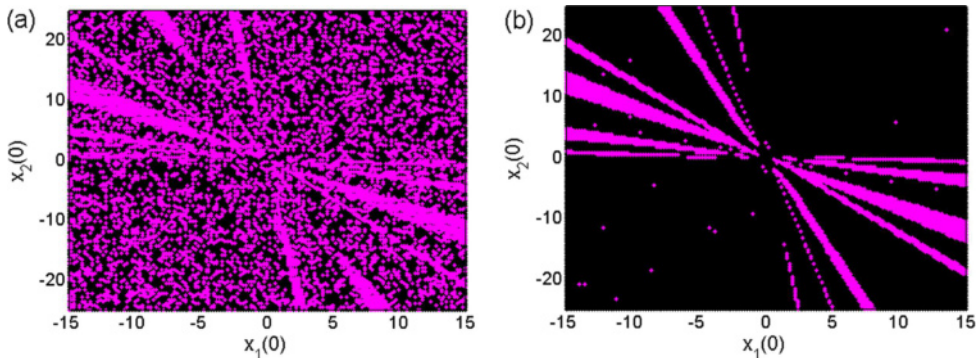


Fig. 7. Section of basins of attraction of coexisting quasiperiodic orbit (magenta) and hyperchaotic (black) attractors in (a) and basins of attraction of coexisting period-1 limit cycle (magenta) and hyperchaotic (black) attractors in (b) shown in Figures 6a and 6b for null initial conditions for other state variables.

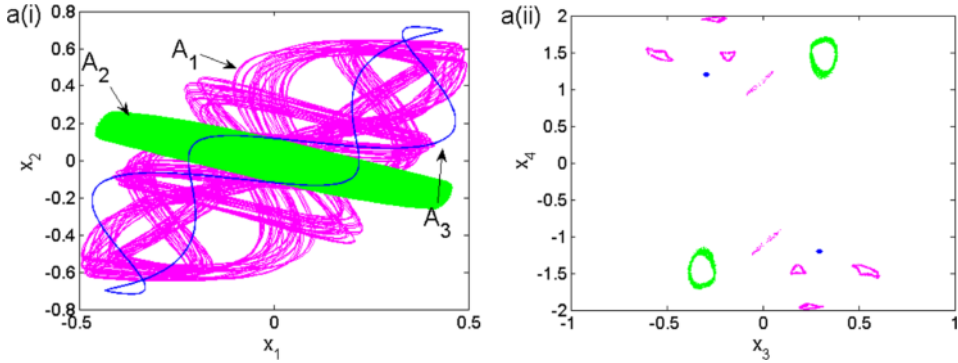


Fig. 8. Coexistence of three symmetric attractors with different shape for $w_{22} = 1.58$, Initial conditions $(x_1(0), x_2(0), x_3(0), x_4(0))$ are $(0, 1.68, 0, 0)$, $(0, 1, 0, 0)$ and $(0, 2, 0, 0)$ respectively for A_1, A_2 and A_3 with their corresponding double sided Poincaré section.

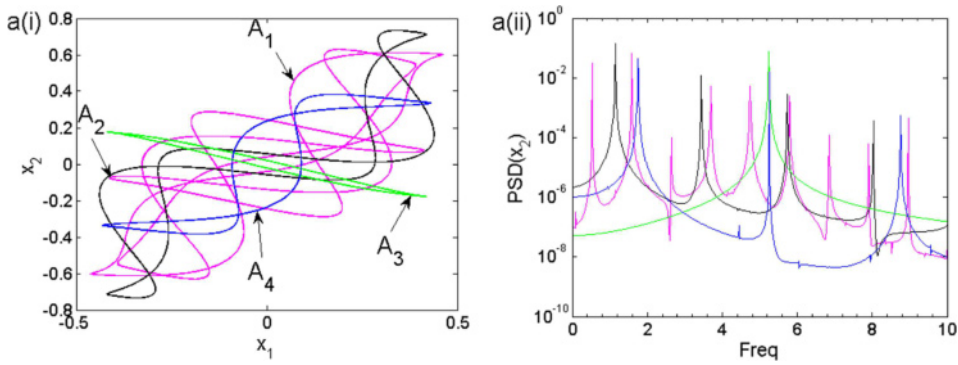


Fig. 9. Coexistence of four symmetric attractors with different shape for $w_{22} = 1.40$, Initial conditions $(x_1(0), x_2(0), x_3(0), x_4(0))$ are $(0, 2, 0, 0)$, $(0, 0.8, 0, 0)$, $(0, 1, 0, 0)$ and $(0, 0.4, 0, 0)$ respectively for A_1, A_2, A_3 and A_4 with their corresponding frequency spectra.

coexistence of period-1 limit cycle with two quasiperiodic orbits of different shapes and their corresponding double-sided Poincaré section in Figure 8a(ii).

In the same line Figure 9a(i) shows the coexistence of four stable states of different topological forms and their corresponding frequency spectra in Figure 9a(ii). Figure 10 represents samples of basins of attraction showing different domains initial conditions in which attractors of Figure 8a respectively Figure 9a can be captured. For example, in Figure 10a the attractor A_1 is represented in cyan, A_2 in yellow and A_3 in blue. In the same line, Figure 10b enables us to see the domain of initial conditions associated with the various coexisting attractors of Figure 10a. It is important to stress that the network addressed in this work possesses rich dynamics since it displays a multitude of coexistence of symmetrical orbits including, periodic, quasi-periodic, chaotic and hyperchaotic one in contrast to the coexistence of pair of symmetrical orbits or coexistence of asymmetrical orbits generally four in the literature [14,15,23,24,28].

Based on the obtained result, we would like to stress that, to the best of the author’s knowledge, the phenomenon of the coexistence of up to four symmetrical attractors obtained in this work is rarely found in the literature. Particularly in Hopfield neural network, this is the first report focused on the coexistence of multiple attractors in a HHNN.

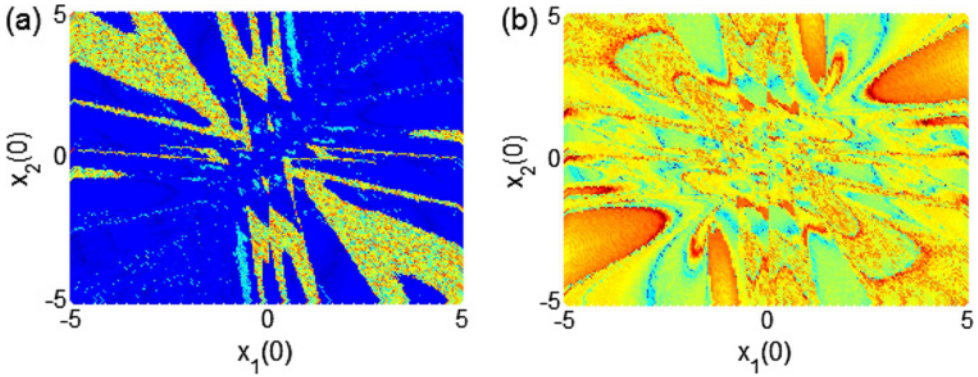


Fig. 10. Section of basins of attraction of coexisting quasiperiodic orbits (cyan, yellow) with an periodic orbit (blue) in (a) and basins of attraction of coexisting of four periodic orbits in (b) as shown in Figures 8 and 9, for null initial conditions for other state variables.

4 PSpice based simulations

4.1 Implementation of the proposed HNNs

Another approach to explore the dynamics of the equation (3) is to construct an analog computer.

Such a method is helpful to show the feasibility of the mathematical model (3) [43–45]. More interestingly, the analog computer offers the possibility to confirm previous results by simply changing the values of a control resistor. It also provides the possibility to introduce wished initial values of capacitors. The main goal of this section is to design and simulate an appropriate analog computer of the mathematical model (3). The circuit in Figure 11 has been designed following the approach of analog computer based on Miller integrators using operational amplifiers, capacitors, resistors. The neuron state variables x_j ($j = 1, 2, 3, 4$) of the system (3) are associated with the voltages across the capacitors C_1, C_2, C_3 and C_4 respectively. As a result, the circuit in Figure 11 is associated by the following evolution equations:

$$\begin{cases} C_1 \frac{dX_1}{dt} = -\frac{1}{R} X_1 + \frac{1}{R_{11}} \tanh(X_1) + \frac{1}{R_{12}} \tanh(X_2) - \frac{1}{R_{13}} \tanh(X_3) - \frac{1}{R_{14}} \tanh(X_4) \\ C_2 \frac{dX_2}{dt} = -\frac{1}{R} X_2 + \frac{1}{R_{22}} \tanh(X_2) + \frac{1}{R_{23}} \tanh(X_3) \\ C_3 \frac{dX_3}{dt} = -\frac{1}{R} X_3 + \frac{1}{R_{31}} \tanh(X_1) - \frac{1}{R_{32}} \tanh(X_2) + \frac{1}{R_{33}} \tanh(X_3) \\ C_4 \frac{dX_4}{dt} = -\frac{1}{R_{40}} X_4 + \frac{1}{R_{41}} \tanh(X_1) + \frac{1}{R_{44}} \tanh(X_4) \end{cases} \quad (21)$$

where $X_1, X_2, X_3,$ and X_4 are the voltage across capacitors C_1, C_2, C_3 and C_4 with $C_1 = C_2 = C_3 = C_4 = C = 10 \text{ nF}, t = \tau RC, R = 10 \text{ K}\Omega, R_C = 1 \text{ K}\Omega, R_0 = 0.52 \text{ K}\Omega, R_{11} = \frac{R}{|w_{11}|} = 10 \text{ K}\Omega, R_{12} = \frac{R}{|w_{12}|} = 20 \text{ K}\Omega, R_{13} = \frac{R}{|w_{13}|} = 3.333 \text{ K}\Omega, R_{14} = \frac{R}{|w_{14}|} = 10 \text{ K}\Omega, R_{23} = \frac{R}{|w_{23}|} = 3.333 \text{ K}\Omega, R_{31} = \frac{R}{|w_{31}|} = 3.333 \text{ K}\Omega, R_{32} = \frac{R}{|w_{32}|} = 3.333 \text{ K}\Omega, R_{33} = \frac{R}{|w_{33}|} = 10 \text{ K}\Omega, R_{40} = \frac{R}{|100|} = 0.1 \text{ K}\Omega, R_{41} = \frac{R}{|w_{41}|} = 0.1 \text{ K}\Omega, R_{22} = \frac{R}{|w_{22}|}$ and $R_{44} = \frac{R}{|w_{44}|}$ are tuneable.

The nonlinear neuron activation function is built-in Figure 11b using resistors, transistors, Op. Amp and a constant current source [34]. Here the value of the constant current source I_0 is 1.1 mA. Note that this constant current source can be implemented physically by the approach of Bao and collaborators [14,15]. The constructed

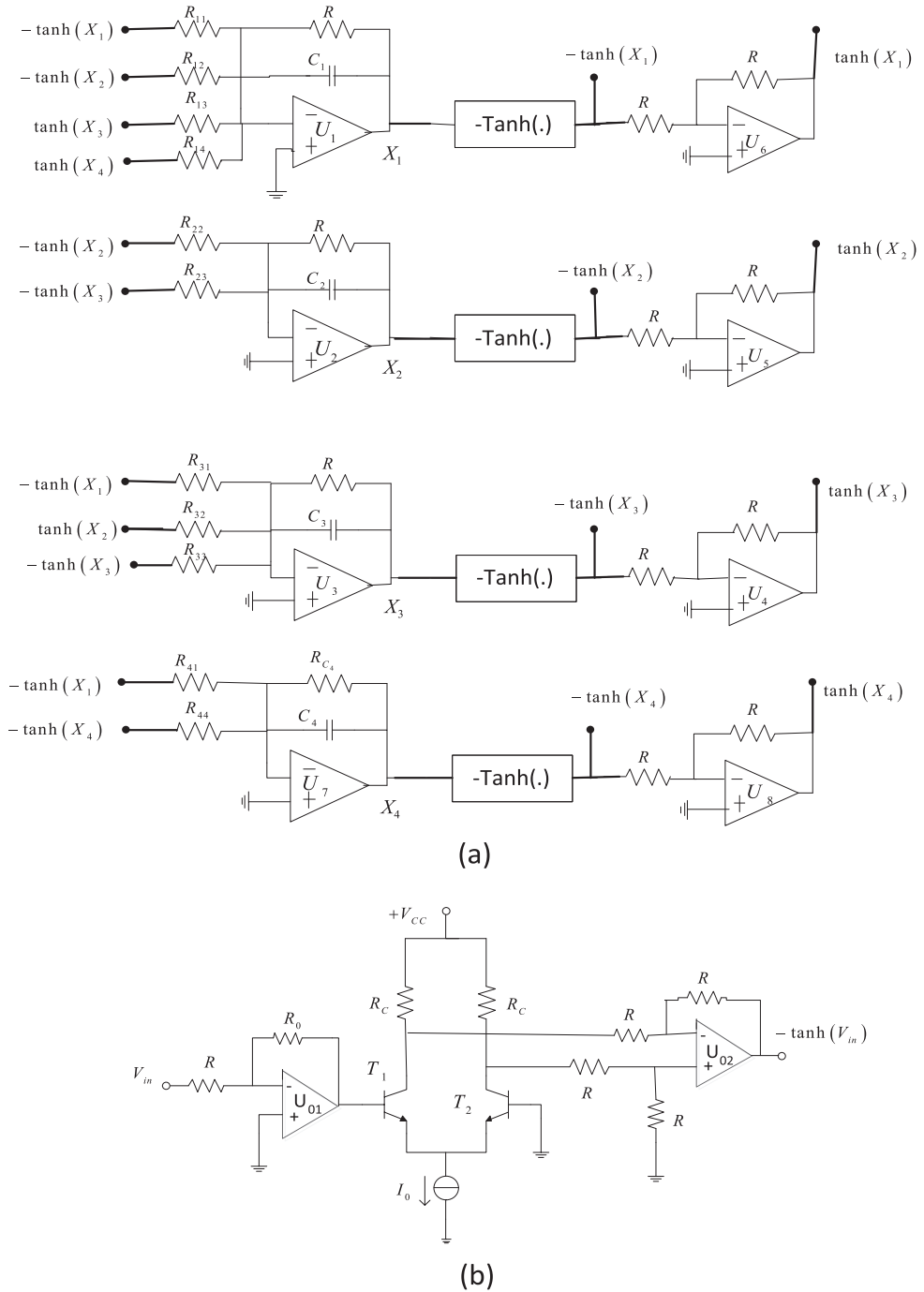


Fig. 11. Circuit realization of the hyperchaotic Hopfield neural network.

circuit is implemented in the electronic simulation package OrCAD. Figure 12 displays some two-dimensional projection of the HHNN in the various planes. From these figures, no form of synchronization is observed between any state variables thus, the possibility of conservative quantities is to exclude.

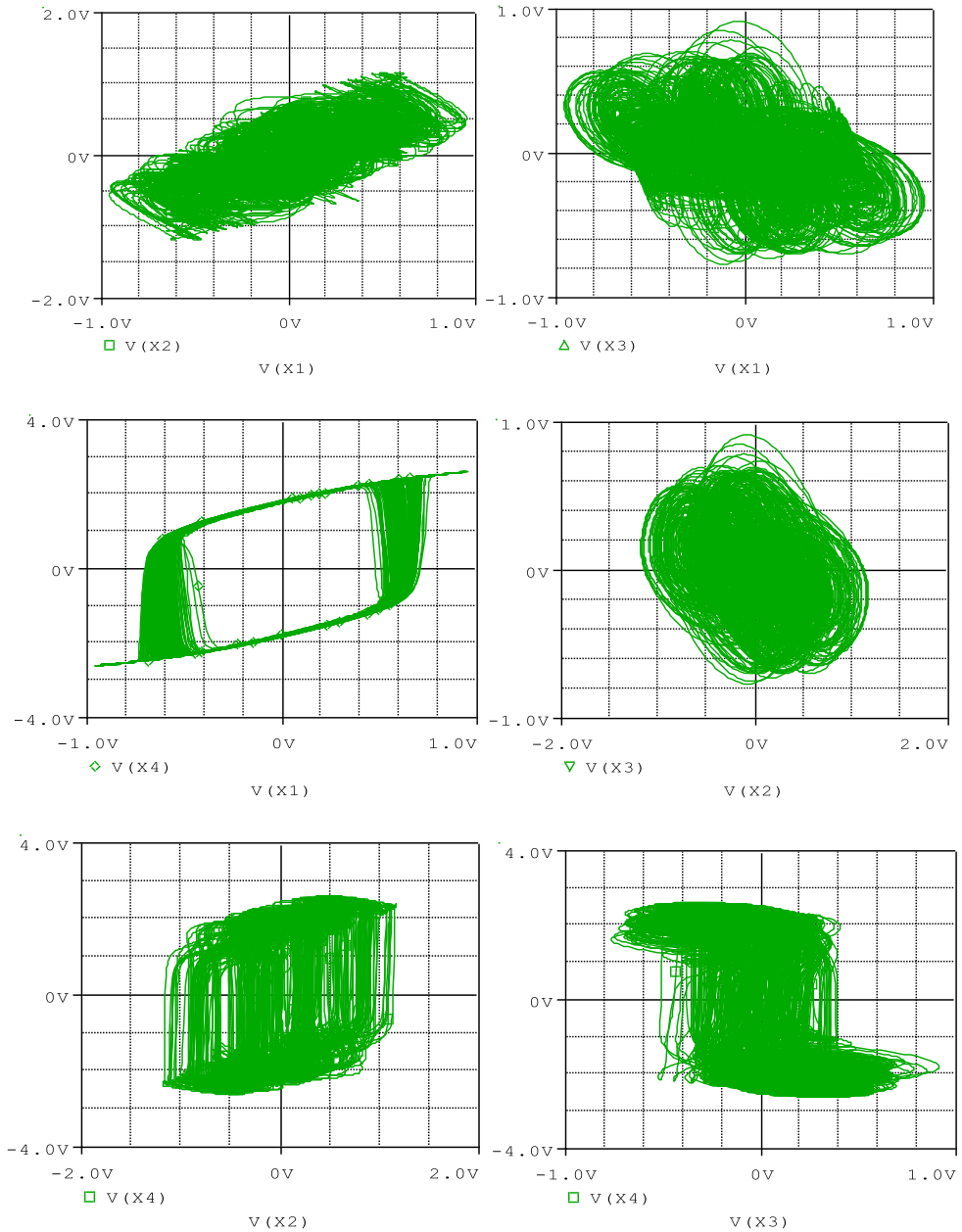


Fig. 12. PSpice simulations results showing 2D projection of the hyperchaotic attractors in the various plane for $R_{44} = 0.05263\text{ k}\Omega$ and $R_{22} = 5\text{ k}\Omega$. Initial conditions $(X_1(0), X_2(0), X_3(0), X_4(0))$ are $(0\text{ V}, 1\text{ V}, 0\text{ V}, 0\text{ V})$.

4.2 Observation of multiple attractors using PSpice

The PSpice simulations have also confirmed the possibility of the coexistence of multiple stable states observed during the theoretical analysis of the HHNN model.

In Figure 13, we present PSpice simulation results showing coexistence of two attractors including a hyperchaotic attractor and period limit cycle in the circuit

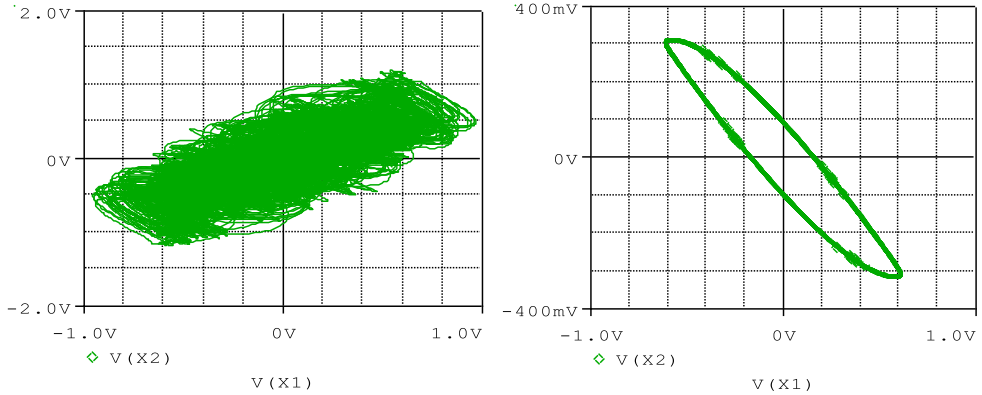


Fig. 13. PSpice simulations results showing coexistence of a symmetric Hyper-chaotic attractors and a symmetric period one limit cycle for $R_{44} = 0.05263\text{ k}\Omega$ and $R_{22} = 5\text{ k}\Omega$. Initial conditions $(X_1(0), X_2(0), X_3(0), X_4(0))$ are $(0\text{ V}, 1\text{ V}, 0\text{ V}, 0\text{ V})$ and $(0\text{ V}, 2.24\text{ V}, 0\text{ V}, 0\text{ V})$ respectively.

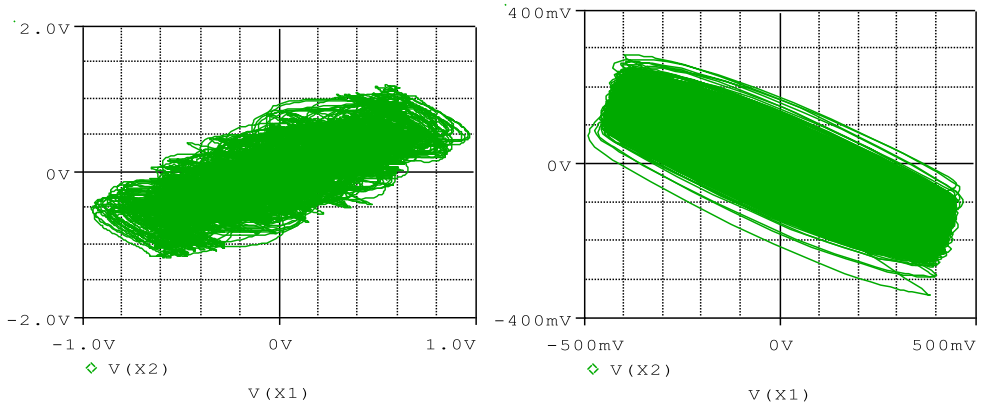


Fig. 14. PSpice simulations results showing coexistence of a symmetric Hyper-chaotic attractors and a symmetric torus for $R_{44} = 0.056\text{ k}\Omega$ and $R_{22} = 5\text{ k}\Omega$. Initial conditions $(X_1(0), X_2(0), X_3(0), X_4(0))$ are $(0\text{ V}, 1\text{ V}, 0\text{ V}, 0\text{ V})$ and $(0\text{ V}, 2.24\text{ V}, 0\text{ V}, 0\text{ V})$ respectively.

mimicking the dynamical behaviour of the HHNN model. Each attractor is obtained for $R_{44} = 0.05263\text{ k}\Omega$ and $R_{22} = 5\text{ k}\Omega$. In the same line, Figure 14 displays the coexistence of two attractors, including a chaotic attractor and a quasi-periodic orbit (two torus) using two different initial conditions.

In the same manner, the coexistence of three and four disconnected symmetric attractors, is presented in Figures 15 and 16. Figures 15 shows the coexistence of two quasiperiodic orbits and a symmetric period -1 limit cycle, obtained by starting from three different initial conditions. Whereas Figure 16: shows the coexistence of four different symmetric attractors with different stating from four different initial conditions. It is good to mention that, minor differences can be observed between values of resistance obtained from PSpice simulation and the one obtained with Turbo Pascal. Such discrepancy can be assigned to computational errors of each integration scheme adopted. In this section, PSpice based simulations have been successfully used to support previous theoretical predictions. The initial condition is very important in systems exhibiting coexistence of multiple stable states. In software simulations like PSpice, the modification initial condition consists to change the initial voltage of the

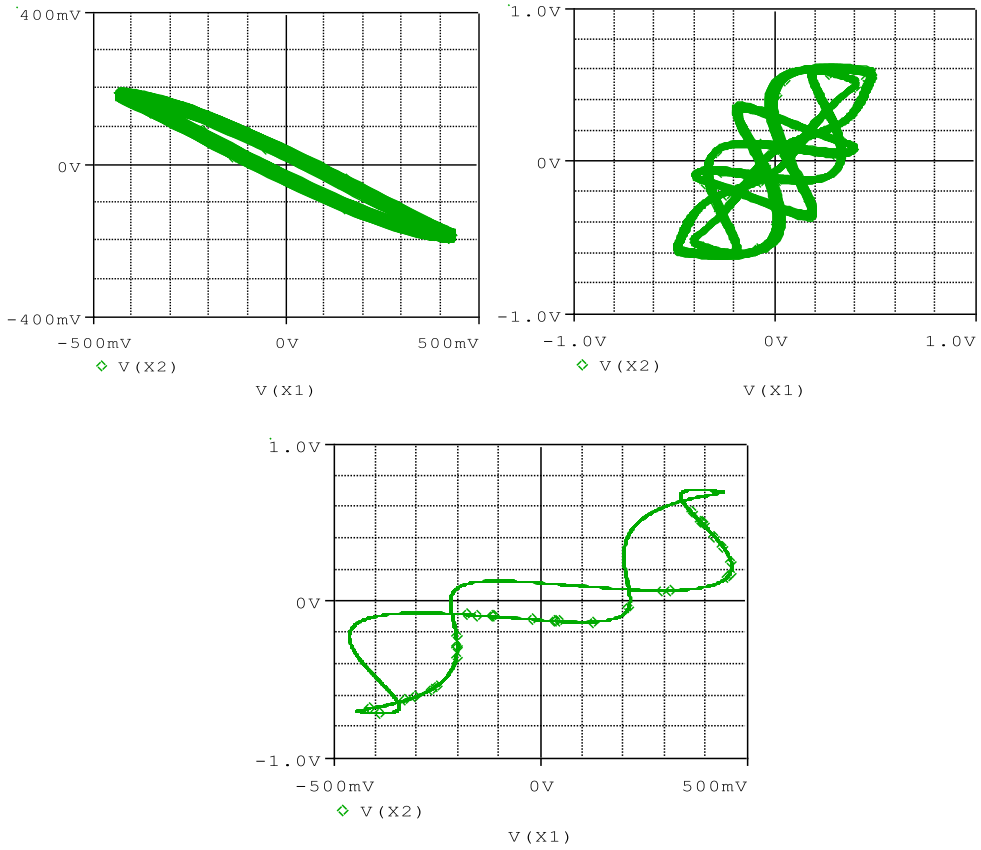


Fig. 15. PSpice simulations results showing coexistence of three attractors with different topologies for $R_{44} = 0.05882\text{ k}\Omega$ and $R_{22} = 6.33\text{ k}\Omega$. Initial conditions $(X_1(0), X_2(0), X_3(0), X_4(0))$ are $(0\text{ V}, 1.1\text{ V}, 0\text{ V}, 0\text{ V})$, $(0\text{ V}, 0.1\text{ V}, 0\text{ V}, 0\text{ V})$ and $(0\text{ V}, 0.5\text{ V}, 0\text{ V}, 0\text{ V})$ respectively.

capacitors or initial current of inductors. This is achieved in hardware experiments by switching on and off the power supply. This technique is very simple although the user has no information about initial conditions used to start the system. The second technique is very complex because the user needs to build a circuit for reinitializing initial conditions before carrying out the experimental work [46].

5 Conclusion

This paper was focused on the dynamic analysis of a hyperchaotic Hopfield neural network in which, multiple bifurcation modes, as well as multiple attractors coexist. The properties of the model including the stability of the unique stationary point, dissipation, and condition of the existence of an attractor were addressed. Investigations have revealed that, the considered HHNN displays some complex nonlinear phenomena such as quasi-periodic orbits, periodic orbits, chaos, hyperchaotic orbits, and coexistence of self-excited attractors (e.g. coexistence of two, three and four disconnected stable states) for the same set of the synaptic weight matrix starting from different initial conditions. These complex phenomena reported in this contribution have been tracked using traditional nonlinear diagnostic tools such as phase

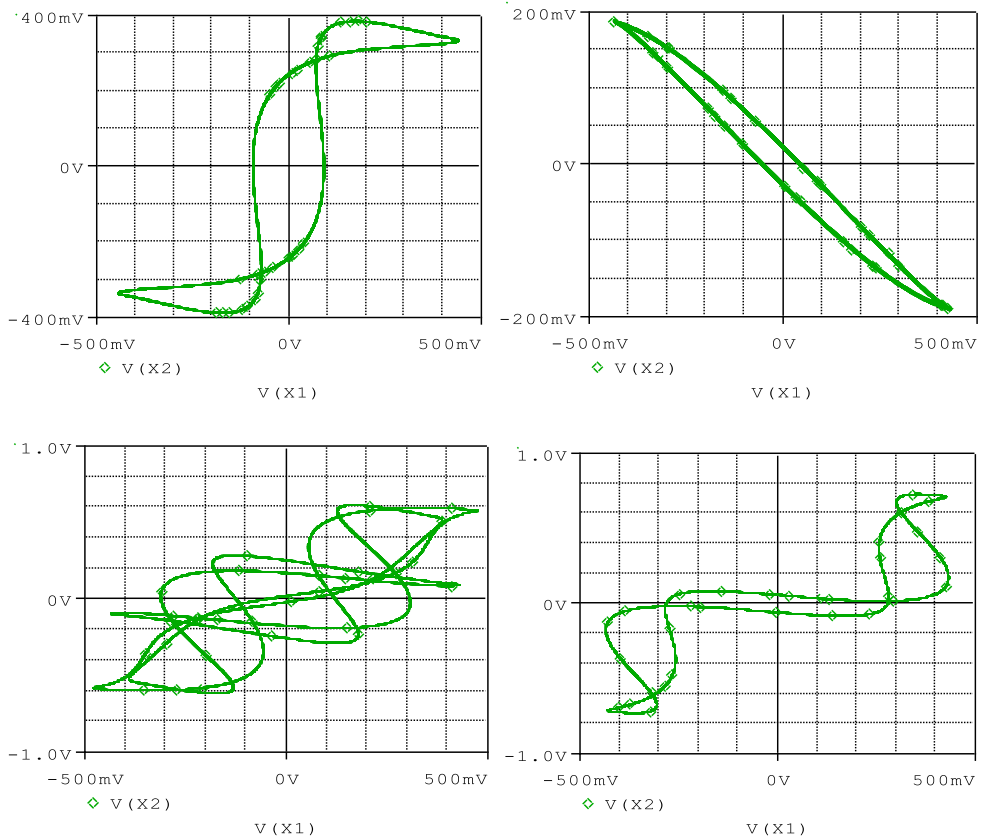


Fig. 16. PSpice simulation results showing coexistence of three attractors with different topologies for $R_{44} = 0.05882 \text{ k}\Omega$ and $R_{22} = 7.14 \text{ k}\Omega$. Initial conditions $(X_1(0), X_2(0), X_3(0), X_4(0))$ are $(0 \text{ V}, 0.5 \text{ V}, 0 \text{ V}, 0 \text{ V})$, $(0 \text{ V}, 1.1 \text{ V}, 0 \text{ V}, 0 \text{ V})$, $(0 \text{ V}, 2 \text{ V}, 0 \text{ V}, 0 \text{ V})$ and $(0 \text{ V}, 2.6 \text{ V}, 0 \text{ V}, 0 \text{ V})$ respectively.

portraits, bifurcation diagrams, and graph of Lyapunov exponents, frequency spectra, two-parameter bifurcation diagrams and basins of attractions. Finally, the results of theoretical/numerical analyses were perfectly supported using PSpice based simulations. The control of the multistability in hyperchaotic Hopfield neural network with coexisting attractors (up to four attractors) represents the topic of our future research works.

The authors would like to thank the Editor and unanimous reviewers for their comments and suggestions that helped to greatly improve the presentation of the present manuscript.

Author contribution statement

The authors declare that each of the five authors equally contributed to both the scientific contents and writing of this manuscript.

References

1. S.H. Strogatz, *Nonlinear dynamics and chaos*, studies in nonlinearity (1994)
2. A. Dutta, P.K. Gupta, Chin. J. Phys. **56**, 1045 (2018)
3. W. Horton, R.S. Weigel, J.C. Sprott, Phys. Plasma **8**, 2946 (2001)
4. W. Horton, I. Doxas, J. Geophys. Res. **103**, 4561 (1998)
5. A. Khan, S. Kumar, Int. J. Dyn. Control **7**, 536 (2019)
6. B. Xin, J. Zhang, Nonlinear Dyn. **79**, 1399 (2015)
7. J.A.M. Borghans, G. DuPont, A. Goldbeter, Biophys. Chem. **66**, 25 (1997)
8. U. Güçlü, M.A.J. van Gerven, Front. Comput. Neurosci. **11**, 1 (2017)
9. Q. Li, X.S. Yang, F. Yang, Neurocomputing **67**, 275 (2005)
10. M.F. Danca, N. Kuznetsov, Chaos Solitons Fractals **103**, 144 (2017)
11. S. Wieczorek, B. Krauskopf, D. Lenstra, Opt. Commun. **172**, 279 (1999)
12. A. Gavrielides, V. Kovanis, P.M. Varangis, T. Erneux, G. Lythe, Quantum Semiclassical Opt. **9**, 785 (1997)
13. J. Ohtsubo, *Semiconductor Lasers*, Springer Series in Optical Sciences (2007)
14. B. Bao, H. Qian, Q. Xu, M. Chen, J. Wang, Y. Yu, Front. Comput. Neurosci. **1**, 1 (2017)
15. B. Bao, H. Qian, J. Wang, Q. Xu, M. Chen, H. Wu, Y. Yu, Nonlinear Dyn. **90**, 2359 (2017)
16. J. Kengne, Nonlinear Dyn. **87**, 363 (2017)
17. Z.T. Njitacke, J. Kengne, H.B. Fotsin, A.N. Negou, D. Tchiotso, Chaos Solitons Fractals **91**, 180 (2016)
18. J. Kengne, Z.T. Njitacke, A.N. Negou, M.T. Fouodji, H.B. Fotsin, Int. J. Bifurc. Chaos **25**, 1550052 (2015)
19. J. Kengne, Z.T. Njitacke, H.B. Fotsin, Nonlinear Dyn. **83**, 751 (2016)
20. Z.T. Njitacke, J. Kengne, L. Kamdjeu Kengne, Chaos Solitons Fractals (in Press)
21. J. Kengne, Z.T. Njitacke, H.B. Fotsin, Commun. Nonlinear Sci. Numer. Simul. **36**, 29 (2016)
22. J. Kengne, Z.T. Njitacke, V.T. Kamdoum, A.N. Negou, Interdiscip. J. Nonlinear Sci. **25**, 103126 (2015)
23. Z.T. Njitacke, J. Kengne, H.B. Fotsin, Int. J. Dyn. Control **7**, 36 (2019)
24. Z.T. Njitacke, J. Kengne, Int. J. Electron. Commun. (AEÜ) **93**, 242 (2018)
25. Q. Lai, A. Akgul, C. Li, G. Xu, Ü. Çavusoglu, Entropy **21**, 12 (2018)
26. Q. Lai, B. Norouzi, F. Liu, Chaos Solitons Fractals **114**, 230 (2018)
27. Q. Lai, C. Chen, X.W. Zhao, J. Kengne, C. Volos, IEEE Access **7**, 24051 (2019)
28. Q. Lai, P.D.K. Kuate, F. Liu, H. H.-C. Iu, IEEE Trans. Circuits Syst. II: Express Briefs, <http://doi.org/10.1109/TCSII.2019.2927371>
29. B. Bao, C. Chen, H. Bao, X. Zhang, Q. Xu, M. Chen, Int. J. Bifurc. Chaos **29**, 1930010 (2019)
30. K. Rajagopal, J.M. Munoz-Pacheco, V.T. Pham, D.V. Hoang, F.E. Alsaadi, F.E. Alsaad, Eur. Phys. J. Special Topics **227**, 811 (2018)
31. J.J. Hopfield et al., Proc. Natl. Acad. Sci. USA **81**, 3088 (1984)
32. G. Pajeras, J.M. Cruz, J. Aranda, Pattern Recognit. **31**, 561 (1998)
33. J. Yang, L.D. Wang, Y. Wang, T.T. Guo, Neurocomputing **227**, 142 (2016)
34. Z.T. Njitacke, R.L. Tagne Mogue, J. Kengne, M. Kountchou, H.B. Fotsin, Iran. J. Sci. Technol. Trans. Electr. Eng. **44**, 413 (2020)
35. R.C. Hilborn, *Chaos and nonlinear dynamics: an introduction for scientists and engineers* (Oxford University Press on Demand, 2000)
36. H.S. Nik, S. Effati, J. Saberi-Nadjafi, Complexity **20**, 30 (2015)
37. J.P. Singh, B.K. Roy, Nonlinear Dyn. **92**, 373 (2017)
38. A. Wolf, J.B. Swift, H.L. Swinney, J.A. Vastano, Physica D **16**, 285 (1985)
39. C. Li, Y. Xu, G. Chen, Y. Liu, J. Zheng, Nonlinear Dyn. **95**, 1245 (2019)
40. Z. Gu, C. Li, H.H.C. Iu, F. Min, Y. Zha, Eur. Phys. J. B **92**, 221 (2019)
41. C. Li, J.C. Sprott, Int. J. Bifurc. Chaos **24**, 1450034 (2014)
42. A.N. Pisarchik, U. Feudel, Phys. Rep. **540**, 167 (2014)
43. J. Kengne, V.R. Folifack Signing, J.C. Chedjou, G.D. Leutcho, Int. J. Dyn. Control **6**, 468 (2018)

44. Z.T. Njitacke, J. Kengne, A.N. Negou, *Optik* **130**, 356 (2017)
45. V.T. Pham, S. Jafari, S. Vaidyanathan, C. Volos, X. Wang, *Sci. Chin. Tech. Sci.* **59**, 358 (2015)
46. M.S. Patel, U. Patel, A. Sen, G.C. Sethia, C. Hens, S.K. Dana, U. Feudel, K. Showalter, C.N. Ngonghala, R.E. Amritkar, *Phys. Rev. E* **89**, 022918 (2014)